The Astrophysical Journal, 790:76 (13pp), 2014 July 20 doi:10.1088/0004-637X/790/1/76

DWARF GALAXIES IN THE HALO OF NGC 891

Earl Schulz
60 Mountain Road, North Granby, CT 06060, USA; earlschulz@gmail.com
Received 2014 May 12; accepted 2014 June 4; published 2014 July 7

ABSTRACT

We report the results of a survey of the region within 40 arcmin of NGC 891, a nearby nearly perfectly edge-on spiral galaxy. Candidate "non-stars" with diameters greater than 15 arcsec were selected from the GSC 2.3.2 catalog and cross-comparison of observations in several bands using archived *GALEX*, DSS2, *WISE*, and Two Micron All Sky Survey images identified contaminating stars, artifacts, and background galaxies, all of which were excluded. The resulting 71 galaxies, many of which were previously uncataloged, comprise a size-limited survey of the region. A majority of the galaxies are in the background of NGC 891 and are for the most part members of the A347 cluster at a distance of about 75 Mpc. The new finds approximately double the known membership of A347, previously thought to be relatively sparse. We identify a total of seven dwarf galaxies, most of which are new discoveries. The newly discovered dwarf galaxies are dim and gas-poor and may be associated with the previously observed arcs of red giant branch halo stars in the halo and the prominent H I filament and the lopsided features in the disk of NGC 891. Several of the dwarfs show signs of disruption, consistent with being remnants of an ancient collision.

Key words: galaxies: clusters: individual (NGC 891) – galaxies: dwarf – galaxies: groups: individual (A347) – surveys

Online-only material: color figures, extended figure

1. INTRODUCTION

Several continuing surveys are underway to find and catalog galaxies in the Local Volume (LV), defined as the region $D < 10$ Mpc. Kaisina et al. (2012) describes the latest version of the Karachentsev et al. (2004) catalog of galaxies of the LV which now contains more than 800 galaxies. The catalog is complete to nearly 100% for galaxies within 2 Mpc and is about 70%–80% complete within 8 Mpc. The inventory of dwarfs within 10 Mpc is much more uncertain and there have been several recent efforts to improve the galaxy census in this region; see especially Gil de Paz et al. (2007), Karachentsev et al. (2007), Huchtmeier et al. (2009), Karachentsev & Kaisin (2010), and Whiting et al. (2007). Most recently, McConnachie (2012) presented observational data for all of the approximately 100 dwarf galaxies in the Local Group for which $D < 3$ Mpc.

More than 80% of the LV galaxies are dwarfs and nearly all of the undetected galaxies must be dwarf irregular (dIrr) galaxies and dwarf spheroidal (dSph) galaxies which are the most challenging to detect. dSph galaxies are small (300 pc $\leqslant D \leqslant$ 1000 pc) and faint ($M_V > -14$) and are morphologically distinct from larger galaxies. dSph galaxies are very gas-poor and do not possess structures such as a spiral arms or bulges and do not have a discernable nucleus. dSph galaxies are very dim with surface brightness in the range $24 \leqslant \mu_B \leqslant 31$. dIrr galaxies are somewhat larger and brighter than dSph galaxies and are distinguished from dSph galaxies by having a much greater gas content and by their characteristic appearance caused by "lumpy" star forming regions.

dSph galaxies are usually found within about 100 kpc of a larger galaxy whereas dIrr are usually undisturbed and more distant from the nearest large galaxy. This is evidence that the two categories may overlap and that some dSph galaxies may be dIrr galaxies which have been stripped of gas by interaction with the halo gas of a larger galaxy.

1.1. Streams and Dwarfs in the Halo of NGC 891

In this paper, we are concerned with dSph galaxies near NGC 891. NGC 891 is a nearby nearly perfectly edge-on ($\theta > 89.^\circ8$) spiral galaxy which is classified as Sb/SBb and is a member of the NGC 1023 group. NGC 891 resembles the Milky Way (MW) galaxy and has been observed in many wavelengths. We take the distance to NGC 891 to be 9.8 Mpc which is consistent with recent surface brightness fluctuation and tip of the red giant branch measurements as given in Tikhonov & Galazutdinova (2005) so that $1'' \approx 47.5$ pc. The heliocentric velocity of NGC 891 is $V_0 = 528\,\mathrm{km\,s^{-1}}$, suggesting a peculiar motion of about $-180\,\mathrm{km\,s^{-1}}$.

NGC 891 is near to the Galactic plane at latitude $b_{\mathrm{gal}} = -17^\circ$ and is very near to the supergalactic plane at $b_{\mathrm{SG}} = -5^\circ$. The foreground extinction toward NGC 891 is .28 mag in B which is significant but, even so, detailed observations in the region are possible.

Mouhcine et al. (2010) presents evidence of an ancient accretion event which affected NGC 891. They find features which extend well into the halo including a number of arcing loops extending to about 30 kpc to the east of the disk and 40 kpc to the west. The loops appear to connect and show high metallicity and ages greater than a few gigayears. Tidal streams of this sort are quite common in the LV. Martínez-Delgado et al. (2010), for instance, observed eight spiral galaxies using very deep ($\mu_V \sim 28.5$ mag arcsec^{-2}) wide-field imaging and found that six of the galaxies had previously undetected stellar structures extending out to ~30 kpc.

Oosterloo et al. (2007) also found evidence of an accretion event: a large gas filament which extends out to about 22 kpc above the plane of the galaxy contains about $1.2 \times 10^9\ M_\odot$ of H I. Oosterloo et al. (2007) performs a simple calculation which shows that it is unlikely that this large amount of gas could have been expelled by a galactic fountain type of mechanism and must therefore be due to an accretion event. Finally, Shih & Méndez (2010) found asymmetries in the distribution of planetary nebula of NGC 891 which they take as evidence of a collision or fly-by interaction.

If the disturbances to NGC 891 were caused by a collision with another galaxy, then there should be nearby evidence of the disrupting galaxy. Oosterloo et al. (2007) proposed that the gas-rich dIrr galaxy UGC 1807, which is 29′ distant from

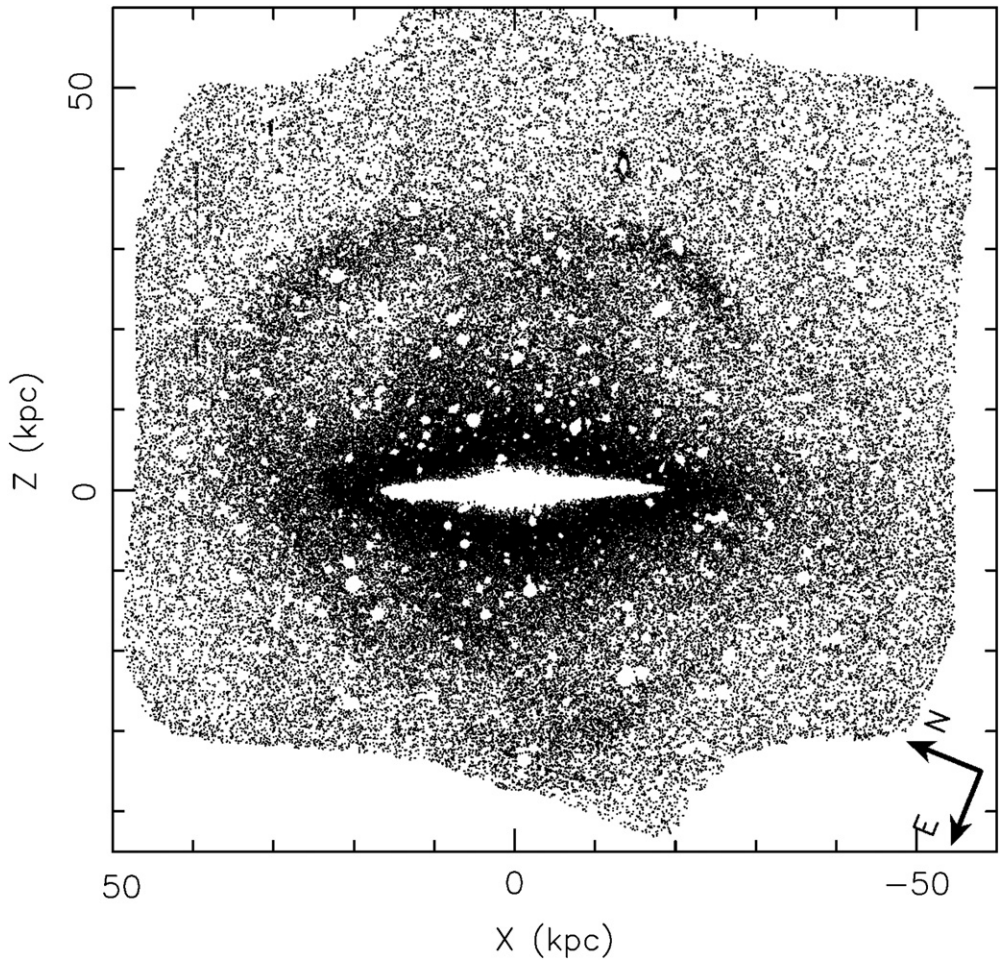

Figure 1. Overdensities of RGB stars in the halo of NGC 891 define streams and loops which may be due to one or more accretion events. A feature at a height of ~40 kpc above the disk is centered on the dSph galaxy HFLLZOA F172. This figure is reproduced from Mouhcine et al. (2010) with permission.

NGC 891, might have caused the disturbance. However, UGC 1807 appears to be undisturbed and shows no signs of a recent interaction and so there is reason to suppose that even if UGC 1807 was the original disrupting galaxy there might be one or more dwarf galaxies in the near vicinity on NGC 891 consisting of tidal remnants of the original collision which account for the continuing disturbances.

The panoramic view of the halo region of NGC 891 presented in Mouhcine et al. (2010) was the impetus for the search presented here and their Figure 1. Mouhcine et al. (2010) used the Subaru Prime Focus Camera on the 8.2 m Subaru Telescope to image the brightest 2 mags of red giant branch (RGB) stars in the outer regions of NGC 891. The images were processed to eliminate foreground stars and other artifacts and to isolate RGB halo stars. The resulting panoramic view of NGC 891 covers a 90 kpc × 90 kpc area and consists of points representing RGB stars in the halo. Unremarked in Mouhcine et al. (2010), the panoramic view shows an overdensity of RGB stars in the NW quadrant of the halo of NGC 891 which frame the tidal radius of dwarf galaxy HFLLZOA F172 (Hau et al. 1995; Trentham & Tully 2009) at a distance of 15′ from NGC 891. Figure 2 is a blowup of a small section of Figure 1, which is reproduced from Mouhcine et al. (2010). Inspection of archived images found that HFLLZOA F172 is certainly a dSph and its association with the halo stars proves that it is in the halo of NGC 891. Archived images of the other galaxies in the Hau et al. (1995) catalog within 1° of NGC 891 were examined and a single additional dSph was found: HFLLZOA F182 at a distance of 20.′1. The remaining galaxies in the Hau et al. (1995) catalog near to NGC 891 were either background galaxies or were ambiguous.

1.2. The Missing Satellite Problem

The cold dark matter (CDM) model predicts that galaxy formation arises by a hierarchical combination of small CDM halos which begins at high redshifts ($z > \sim$100) and is essentially complete by about $z \sim$ 2–3 (White & Rees 1978; White & Frenk 1991). This clustering is purely gravitational and is driven by the dominant CDM component. Baryonic material which falls into the CDM gravitational wells builds the visible structures of the galaxies as gas cools and forms stars in a process which continues to the present day. Simulations predict that the outermost regions of acquired CDM satellites merge with the halo of the accreting galaxy to form a single large CDM halo such as that which is thought to host the MW galaxy. The cores of most of the CDM satellites are predicted to survive and we observe the baryonic portions of these satellites as dwarf galaxies.

The so-called missing satellite problem (Klypin et al. 1999; Moore et al. 1999) is that far fewer dwarf companions of large galaxies are observed than are predicted. For example, a galaxy the size of the MW way is predicted to have several hundred dwarf companions, whereas only 26 have been discovered to date and this discrepancy seems to apply generally. It is possible

Figure 2. Expanded view of a small section of Figure 1 centered at coordinates of $X = 40$ kpc; $Z = -13$ kpc. RGB stars in the halo of NGC 891 outline the tidal radius of the dwarf galaxy HFLLZOA F172.

that the predicted dark matter (DM) subhalos do not, in fact, exist but this would conflict with the concordant model and so much effort is being spent to reconcile the disagreement.

Bullock et al. (2010) summarize the recent work related to the recent discovery of more than two dozen new dwarf companions to the MW and M31. Most of the new dwarfs are fainter than any previously known galaxies with the faintest dwarfs having luminosity of only 10^2–10^4 $L_\odot$, which supports the idea that there is a large population of dwarf galaxies that have not yet been detected. Assuming that the new class of dwarfs can satisfy the numeric deficiency the most pressing problem is to determine the relationship between dwarf luminosity, dwarf baryonic mass, and the mass of the DM subhalo. Currently, there is no useful trend and in some cases the kinetics of the smallest, least luminous, dwarfs imply a DM halo which is as massive as systems 10,000 times more luminous.

A number of studies (e.g., Larson 1974; Dekel & Silk 1986) have shown the processes of supernova heating and the reionization of the universe could have had a strong effect to reduce the baryonic fraction of dwarfs at $z \gtrsim 6$. Later, stochastic effects might have resulted in the situation which seem we seem to see today where some very large halos have not acquired significant baryonic component (Barkana & Loeb 1999). Alternately, Nichols & Bland-Hawthorn (2011) proposes that ram-pressure stripping and super-nova heating combined can account for the observed populations of gas-poor dwarfs within about 270 kpc of their primary. Guo et al. (2010) supports the idea that the abundance of DM halos as a function of their mass is well known and supported by basic theory. They propose that stellar mass as a function of the halo mass is monotonic but not at all linear. Star formation efficiency is much lower for both the highest and the lowest halo mass systems and so we observe a distribution of galaxies which is biased toward middle values.

Boylan-Kolchin et al. (2011) and Boylan-Kolchin et al. (2012) discuss a further complication in that the kinematics of the brightest dwarf satellites of the MW imply a halo density distribution which is much less dense than demanded by theory. The apparent lack of high-mass subhalos might be a more fundamental problem than the numeric deficiency.

The current work contributes to understanding the "missing satellite problem" by providing a dwarf galaxy count for a galaxy similar to the MW. It is part of a growing number of surveys which indicate more and more strongly that there is a basic conflict between theory and observation.

2. A SIZE-LIMITED GALAXY SURVEY

A methodical search for visible galaxies in the vicinity of NGC 891 was undertaken by examining candidates taken from The Guide Star Catalog II (GSC 2.3.2; Lasker et al. 2008). The

GSC 2.3.2 is a deep all-sky catalog derived from the Digitized Sky Surveys, which in turn were created from Palomar and UK Schmidt survey plates, and is based on at least two epochs and three passbands. The catalog classifies objects as one of two types: "stars," which are classified correctly as such with high confidence, and "nonstars" which include not only galaxies but also overlapping images and artifacts such as diffraction spikes near bright stars, halos, etc. In general, "nonstars" are primarily galaxies far from the Galactic plane and primarily blends near the plane. The stellar magnitudes given in GSC 2.3.2 are accurate. However, because the photometric pipeline is tuned for point-like objects, the magnitude of bright galaxies $R_F < 18$ are systematically overestimated. The R_F magnitudes are most affected and were found to be overestimated by as much as several magnitudes.

The candidates were 173 "nonstars" from the GSC 2.3.2 catalog lying within 40′ of NGC 891 (113 kpc at the distance of NGC 891) for which the major axis was greater than 15″. The search region was limited in order to keep the number of candidates to a reasonable total and because *GALEX* observations covered this region.

Each of the candidate "non-stars" was examined by using the NASA *Skyview* utility to generate $1' \times 1'$ false color images from archived data consisting of *GALEX* FUV and NUV images (Martin et al. 2005); DSS2 *R*, *B*, and NIR images; Two Micron All Sky Survey (2MASS) *H*, *J*, and *K* images (Skrutskie et al. 2006); and *WISE W1, W2, W3*, and *W4* images (Wright et al. 2010). In addition, a standard rgb image constructed from *GALEX* NUV, DSS2 *R*, and 2MASS *J* wavelengths proved useful because of the large UV excess exhibited by the dSph galaxies in the sample. These observations in several wavelengths eliminated overlapping images and artifacts with high confidence leaving 71 confirmed galaxies which comprise a complete size-limited survey of the region.

2.1. Distinguishing the Dwarf Galaxies

The goal of the present study is to differentiate foreground dSph galaxies from normally sized galaxies at a much greater distance in the background. This task is similar to that described in Conselice et al. (2002), who defined photometric and structural properties of galaxies in clusters in order to discriminate members of the A426 group (at at distance of 77 Mpc) from background galaxies at distances up to $z = 0.5$. However, it is easier to distinguish dSph galaxies because they are very different in morphology from the larger galaxies whereas the differences which separate cluster galaxies from isolated galaxies are relatively subtle. In addition, the availability of images at many wavelengths is invaluable.

dSph galaxies have diameters in the range of about 200 pc $< D <$ 1,800 pc. By design, the minimum diameter of the survey galaxies is 15″ and the diameter of largest galaxies for which there is no velocity data is about 40″. At the distance NGC 891, this range of angular size corresponds to a range of actual size of about 700 pc $< D <$ 1900 pc compared to a range of actual size of about 5000 pc $< D <$ 15,000 pc at the distance of the A347 cluster. Thus, based on the size, the foreground galaxies consist solely of dSph galaxies, whereas the background galaxies are normally sized: two distinctly different populations.

Since many of the survey galaxies lack measured distances, it is not possible to use absolute magnitude to identify likely dSph galaxies. Instead, we ordered the candidates using an I_N surface brightness metric calculated from the apparent NIR magnitude and angular size as given in the GSC 2.3.2 catalog. Testing showed that this parameter is the best discriminator to sort out foreground from background galaxies, presumably because NIR magnitude is a better measure of stellar surface mass density than the *R* or *B* magnitudes, which show much more scatter. Note that the magnitudes given in GSC 2.3.2 for extended sources are known to be systematically too bright by 2 mag or more and the cataloged radial size (which is the projected radius at which the *R*-magnitude surface brightness reaches the background level) differs significantly from the tidal radius which would be more appropriate for this use. Despite these known errors, the metric is useful because it is a monotonic measure sufficient for the purpose of sorting and comparing the candidates.

The survey galaxies were ordered by I_N surface brightness metric described above and it was found that *none* of the lowest surface brightness candidates $\mu_I > \sim 21.8$ mag arcsec^{-2} showed signs of structure such as spiral arms or a discernable core. In contrast, *all* of the higher surface brightness candidate galaxies for which $\mu_I <\sim 21$ mag arcsec^{-2} showed signs of structure such as spiral arms, and most commonly a distinct core, and so are not dSph galaxies. This is consistent with previous work; see for example Gallagher & Wyse (1994).

Grebel et al. (2003) found that nondetections of H I occur in low-mass dwarfs that are within about 300 kpc of their host. Similarly, Grcevich & Putman (2009) reports that galaxies within about 270 kpc of the MW or Andromeda are undetected in H I (i.e., H I mass is less than about 10^4 $M_\odot$ for MW dwarfs), while those further than 270 kpc are predominantly detected with H I masses in the range 10^5 $M_\odot$ to 10^8 $M_\odot$. The NGC 891 companion dSph galaxies are consistent with this finding in that none of the dSph galaxies near NGC 891 were found by the 2MASX survey and the candidate galaxies which were dimmest in NIR were not detected in 2MASS *J*, *H*, or *K* bands or in *WISE* *W*3 or *W*4 bands which are sensitive to secondary emissions from the dust and gas in the interstellar medium (ISM). The 2MASX survey (Jarrett et al. 2000) extended source sensitivity is about 14.7, 13.9, and 13.1 mag at *J*, *H*, K_s. The detection thresholds were chosen to assure complete detection of galaxies brighter than $K_s \sim 13.5$ and $J \sim 15$ mag away from the Galactic plane and the limit is somewhat brighter close to the plane. Because the lowest surface brightness galaxies are bluer within the NIR bands, the faintest galaxies are observed only in *J*. Some previous surveys of the LV galaxies took candidates from the 2MASX Catalog (e.g., Gil de Paz et al. 2007) and these surveys missed the gas-free dSph galaxies reported here even though they are readily apparent UV and visible wavelengths.

Here we make the assumption that background galaxies are members of the A347 cluster in the background of NGC 891. A347 is at a nominal recession velocity of $V = 5516$ km s^{-1} and is a member of the Perseus-Pisces supercluster. As argued in Trentham & Tully (2009), the void between the LV and the A347 cluster makes it possible to distinguish between the foreground and background galaxies based on morphology with some degree of confidence. Accordingly, a goal of the present study is to differentiate between dSph galaxies in the foreground at a distance of about 9.8 Mpc and background galaxies at a distance of about 72 Mpc or more. In particular, the velocity histogram presented as Figure 4 of Trentham & Tully (2009) supports the assumption that contamination along the line of sight to the A347 cluster is insignificant. The Sakai et al. (2012) catalog identifies a total 37 members of A347, 12 of which are in the region $R \leqslant 40'$ around NGC 891, and the recent 2MRS survey (Huchra et al. 2012) approximately doubles these counts.

Table 1
Galaxies near NGC 891

ID	GSC2.3 ID	R.A./Decl. J2000 (h:m:s) (d:m:s)	Dist (arcmin)	Alt ID	SID (num)	2MX	Vel (kms)	R_F[a] (mag)	BJ[a] (mag)	IN[a] (mag)	Rad[a] (asec)	NIR μ (m/asc2)	Fore
1	NCIA029460	02:24:42+42:49:54	37.44					16.71	17.87	19[b]	10.6	25[b]	F
2	NCIA018969	02:21:12+42:21:50	14.93	HFLLZOA F172				15.76	17.97	18.58	12.1	24.9	F
3	NCIA030805	02:23:35+42:55:27	36.37					16.35	18.20	18.78	11.2	24.8	F
4	NCIA019215	02:24:24+42:21:10	20.49					17.56	18.35	17.98	9.3	23.5	F
5	NBZ5012013	02:20:07+42:45:44	36.56					16.33	16.73	17.95	7.7	23.3	F
6	NCIB031541	02:22:55+41:43:41	37.43					16.08	17.36	17.62	8.4	23.3	F
7	NBZ5012371	02:21:13+42:45:46	28.87	UGC 1807			629	10.22	11.26	14.36	27.6	22.7	F
8	NCIA035836	02:24:05+42:08:15	21.26					15.34	17.44	16.39	10.2	22.5	···
9	NCIA025916	02:24:29+42:38:37	27.83					16.47	17.34	16.96	7.7	22.3	···
10	NCIA030487	02:24:15+42:53:59	38.09					15.50	16.29	16.50	8.8	22.1	···
11	NCIA005660	02:25:14+41:54:47	39.62					15.51	17.33	16.24	8.7	21.9	···
12	NBZ5004290	02:19:50+42:15:52	30.61					14.40	15.64	15.75	10.1	21.8	···
13	NCIA023873	02:24:01+42:32:41	20.03	HFLLZOA F182				12.67	13.69	15.02	13.6	21.7	···
14	NCIA004638	02:23:49+41:53:03	31.24		33			13.26	16.17	14.57	17.6	21.7	···
15	NBZ5003674	02:19:55+42:11:42	30.57					14.53	16.16	15.62	9.5	21.6	···
16	NBZ5015034	02:21:17+42:52:44	34.76	PGC 2187376	2		6,805	13.81	14.97	15.28	9.4	21.3	···
17	NCIA012578	02:25:11+42:07:35	32.10	PGC 2192879	65			15.44	17.45	15.79	7.7	21.2	···
18	NCIA009669	02:24:20+42:02:35	26.95		46		5,680	14.62	16.39	15.43	9.3	21.2	···
19	NCIA010240	02:24:39+42:03:24	29.23		51		5,910	15.13	17.01	15.55	8.3	21.1	···
20	NBZ5004664	02:20:25+42:17:43	23.82	PGC 2196068		Y		12.69	14.44	14.24	15.7	21.1	···
21	NCIA007657	02:21:16+42:00:06	25.23			Y		16.33	19.21	15.68	7.8	21.0	···
22	NCIA010627	02:23:49+42:04:40	21.47					15.32	17.66	15.36	8.2	20.9	···
23	NCIA006643	02:25:13+41:56:42	38.25		66	Y		15.03	17.23	15.34	8.0	20.9	···
24	NCIA010131	02:21:32+42:04:28	19.94					15.28	17.41	15.26	7.7	20.6	···
25	NCIA012182	02:22:21+42:08:00	13.09					15.18	17.04	15.08	7.7	20.5	···
26	NCIA012187	02:25:28+42:06:45	35.29	PGC 2192614		Y		14.59	16.92	14.42	9.1	20.1	···
27	NCIA019867	02:26:03+42:22:08	38.88	PGC 2197501		Y	4,451	14.72	16.22	14.60	7.8	20.0	···
28	NCIA026109	02:25:13+42:38:55	34.57			Y		14.09	15.27	14.52	7.6	19.9	···
29	NCIA016387	02:20:42+42:16:35	20.90			Y		13.38	15.69	13.81	10.1	19.9	···
30	NCIA031935	02:22:28+43:00:49	39.93	PGC 2211100		Y	20,006	13.15	14.50	13.81	10.1	19.9	···
31	NCIA016766	02:24:18+42:16:13	19.94			Y		13.29	15.11	13.53	10.6	19.7	···
32	NCIA029870	02:23:39+42:51:56	33.32	HFLLZOA F179		Y		12.79	14.22	13.41	10.9	19.6	···
33	NCIA010841	02:20:51+42:05:57	24.05	PGC 2192372		Y		13.68	15.45	13.71	9.7	19.6	···
34	NCIA008246	02:23:44+42:00:23	24.43			Y		13.74	15.65	13.95	7.7	19.4	···
35	NCIA031681	02:22:51+42:59:16	38.52	PGC 2210478		Y		12.85	14.45	13.31	10.6	19.4	···
36	NCIA010315	02:20:49+42:05:02	24.97	PGC 2192089				13.19	14.38	13.57	8.3	19.3	···
37	NCIA004881	02:23:46+41:53:38	30.46	PGC 2188688		Y		11.93	15.01	12.36	14.2	19.2	···
38	NCIA027059	02:23:59+42:42:28	26.82	HFLLZOA F181		Y		12.87	14.05	12.91	12.0	19.1	···
39	NCIA031605	02:22:58+42:58:55	38.29	PGC 2210361		Y	20,296	11.69	13.54	12.20	14.7	19.0	···
40	NBZ5010876	02:21:32+42:41:36	23.51	HFLLZOA F176		Y		12.71	12.86	13.04	9.3	19.0	···
41	NCIA027303	02:22:50+42:43:28	22.79	HFLLZOA F210		Y		12.22	13.43	12.58	12.2	18.9	···
42	NCIA029804	02:23:24+42:51:48	32.28	HFLLZOA F178		Y		12.20	13.49	12.58	11.8	18.9	···
43	NCIA004956	02:23:33+41:53:57	29.19	PGC 212966		Y		13.23	15.92	13.05	8.8	18.9	···
44	NCIA006145	02:22:36+41:56:45	24.16	HFLLZOA F187		Y		13.16	15.66	13.01	9.2	18.9	···
45	NCIA001071	02:24:01+42:04:02	23.44	HFLLZOA F191		Y		na	13.80	11.97	15.2	18.6	···
46	NCIA001356	02:21:06+41:49:13	35.59	PGC 8939		Y		11.29	13.83	11.70	13.8	18.5	···
47	NCIA015505	02:24:08+42:13:42	18.95	PGC 2194768		Y		12.15	14.23	11.81	13.7	18.4	···
48	NBZ5000254	02:19:46+42:43:15	38.08	HFLLZOA F170		Y		11.93	13.27	12.11	11.1	18.4	···
49	NCIA000887	02:23:54+42:12:22	17.19	PGC 9101		Y	13,041	11.00	12.71	11.18	16.0	18.3	···
50	NCIA001268	02:24:49+41:54:22	36.56	HFLLZOA F206		Y		11.94	13.91	11.63	14.7	18.3	···
51	NCIA001160	02:23:30+41:59:54	23.51	NGC 2190563	25	Y	6,895	12.54	14.47	12.28	9.7	18.3	···
52	NCIA000452	02:24:32+42:34:45	26.03	PGC 212970		Y	6,661	11.18	12.47	11.35	15.8	18.2	···
53	NCIA001126	02:24:47+42:01:27	31.56	PGC009151	55	Y	6,086	11.02	12.57	10.86	21.5	18.2	···
54	NCIA000277	02:25:10+42:46:33	38.61			Y		10.50	11.80	10.92	17.4	18.1	···
55	NCIA001249	02:23:16+41:55:21	26.74	PGC 212965		Y		12.73	14.63	12.20	9.8	18.1	···
56	NCIA000313	02:23:15+42:43:53	24.27	PGC 2204990		Y		11.60	12.99	11.84	10.3	18.0	···
57	NCIA000956	02:22:50+42:09:29	11.87	PGC 9042	10	Y	6,390	11.50	13.06	11.51	12.1	18.0	···
58	NCIA030617	02:23:03+42:54:45	34.31	PGC 3097117	19	Y	6,895	11.02	12.84	11.10	14.2	17.9	···
59	NCIA001042	02:22:59+42:05:38	16.02	PGC 2192261		Y		10.98	12.83	10.71	18.8	17.9	···
60	NCIA001337	02:23:03+41:50:53	30.53	HFLLZOA F261		Y		11.77	13.69	11.39	12.9	17.9	···
61	NBZ5000678	02:21:24+42:52:34	34.14	PGC 8955	3	Y	6,639	10.03	12.05	10.13	23.9	17.8	···
62	NBZ5000685	02:21:12+42:51:48	34.29	PGC 8948		Y	10,073	10.10	11.82	10.32	19.4	17.8	···
63	NCIA000991[c]	02:25:33+42:08:03	35.87	PGC 2193030		Y	4,451	10.90	12.84	10.67	16.5	17.7	···
64	NCIA000260	02:23:52+42:47:34	30.39	PGC 220681		Y	5,984	10.38	11.74	10.57	15.4	17.6	···
65	NCIA001051	02:25:16+42:05:22	34.00	NGC 906		Y	4,680	8.83	9.99	8.75	34.2	17.5	···

Table 1
(Continued)

ID	GSC2.3 ID	R.A./Decl. J2000 (h:m:s) (d:m:s)	Dist (arcmin)	Alt ID	SID (num)	2MX	Vel (kms)	R_F[a] (mag)	BJ[a] (mag)	IN [a] (mag)	Rad[a] (asec)	NIR μ (m/asc2)	Fore
66	NCIA000248	02:22:18+42:48:19	27.55	PGC 9017		Y	6,354	10.12	11.51	10.11	19.0	17.4	···
67	NCIA001220	02:23:20+41:57:05	25.39	NGC 898		Y	5,495	8.54	9.76	na	41.8	17[b]	···
68	NCIA000407	02:24:44+42:37:23	29.32	UGC 1859		Y	6,087	8.95	10.05	8.41	30.6	16.9	···
69	NCIA001111	02:25:23+42:02:08	36.64	NGC 909		Y	4,978	9.05	10.48	8.54	24.0	16.6	···
70	NCIA001162	02:24:02+41:59:44	26.83	PGC 9108		Y	5,659	9.80	11.13	9.39	16.1	16.5	···
71	NCIA000110	02:23:13+42:59:16	39.07	PGC 212964		Y	6,595	na	na	9.98	8.0	15.6	···

Notes.
[a] This data from the GSC 2.3.2 catalog is affected by relatively large systematic errors.
[b] Estimated.
[c] No. 63 was incorrectly cataloged as a star (type = 0) in GSC2.3.

All but four of the background galaxies for which there are measured velocities lie between 5500 km s^{-1} and 6500 km s^{-1} and there no galaxies in the background of NGC 891 with measured velocities between 630 km s^{-1} and 4450 km s^{-1}.

3. DISCUSSION

Table 1 gives data for the 71 galaxies from the GSC 2.3.2 catalog. Table 1 provides the following information:

Column 1: ID number;
Column 2: GSC 2.3.2 ID;
Column 3: Position (J2000 R.A./Decl.);
Column 4: Distance from NGC 891 (arcmin);
Column 5: Most commonly used alternate ID;
Column 6: ID number if listed in the Sakai et al. (2012) catalog;
Column 7: Indicates if the galaxy is listed in the 2MASX catalog (Jarrett et al. 2000);
Column 8: Radial velocity (km s^{-1}) if available;
Column 9: Apparent R_F magnitude from GSC 2.3.2 (mag);
Column 10: Apparent B_J magnitude from GSC 2.3.2 (mag);
Column 11: Apparent I_N magnitude from GSC 2.3.2 (mag);
Column 12: Semi-major axis from GSC 2.3.2 (arcsec);
Column 13: Calculated NIR surface brightness (mag/arcsec^2);
Column 14: "*F*" indicates that this is a foreground dwarf.

Table 1 identifies seven dwarf companions of NGC 891, all but two of which are new discoveries. Note that the boundary which defines the dwarf galaxies is uncertain by at least 0.5 mag, which might have caused a few of the galaxies in Table 1 to be mis-classified.

Figure 3 provides a set of 13 false color images generated using the Skyview utility for of each of the Table 1 entries. The images are sorted by DSS2 NIR surface brightness in the same way as the Table 1 entries. Each of the images cover a $1' \times 1'$ field of view (FOV) and is centered at the coordinates given in Table 1. The first image of each set is a rgb overlay and the remaining images use linear brightness scaling and a preset false color scheme (the "Stern Special") which was found to best bring out the faintest images. The images are as follows:

1 rgb overlay: *R*, NUV, and *J*;
2 *Galex* FUV 0.155;
3 *Galex* NUV 0.223;
4 DSS2 *B* 0.442;
5 DSS2 *R* 0.647;
6 DSS2 NIR 0.786;
7 2MASS *J* 1.235;
8 2MASS *H* 1.662;
9 2MASS *K* 2.159;
10 *WISE W1* 3.4;
11 *WISE W2* 4.6;
12 *WISE W3* 12;
13 *WISE W4* 22,

where the third column gives the central wavelength of each of the images.

Table 1 and Figure 3 show the trend that the brighter galaxies possess internal structure such as spiral arms and distinct cores whereas the dimmest galaxies do not. A few of the dimmer galaxies, Galaxies No. 5 (NCIA019215) and No. 13 (NBZ5004290), seem to consist of two or three separate bodies spread out over an area of about 30″–40″, suggesting that these dwarfs may consist of tidal remnants which are still coalescing.

Velocity data taken from NED is given for 24 of the candidate galaxies. Most of the background galaxies are seen to be members of the A347 group, except that four galaxies (31, 40, 50, and 63) are apparently located at greater recession velocity, ranging from 10,000 km s^{-1} to 20,000 km s^{-1}.

As indicated in Table 1, 11 of the galaxies were identified by Sakai et al. (2012) as being members of A347. Sakai et al. (2012) used the MOSAIC-1 CCD Imager on the Kitt Peak National Observatory 0.9 m telescope to survey several clusters. The FOV was $59' \times 59'$ and two pointings were made in the A347 region in the background of NGC 891. The survey determined group membership using narrowband filters corresponding to H_α redshifted by various amounts. The pointings in the A347 field used the 120 Å shifted filter which corresponds to $\Delta V \sim 5516$ km s^{-1}.

Thirty-two galaxies were not identified as being in the foreground, do not have measured velocities, and are not included in the Sakai et al. (2012) catalog. Based on morphology and size, most or all of these galaxies are members of the A147 cluster, which approximately doubles the known membership of the cluster.

Figure 4 shows the distribution of the dwarf galaxies relative to NGC 891. The dwarfs appear to be distributed isotropically around NGC 891, the host galaxy. The dSph galaxies which were determined to be companions of NGC 891 showed weak indication in the *WISE W*1 and *W*2 bands which are sensitive to

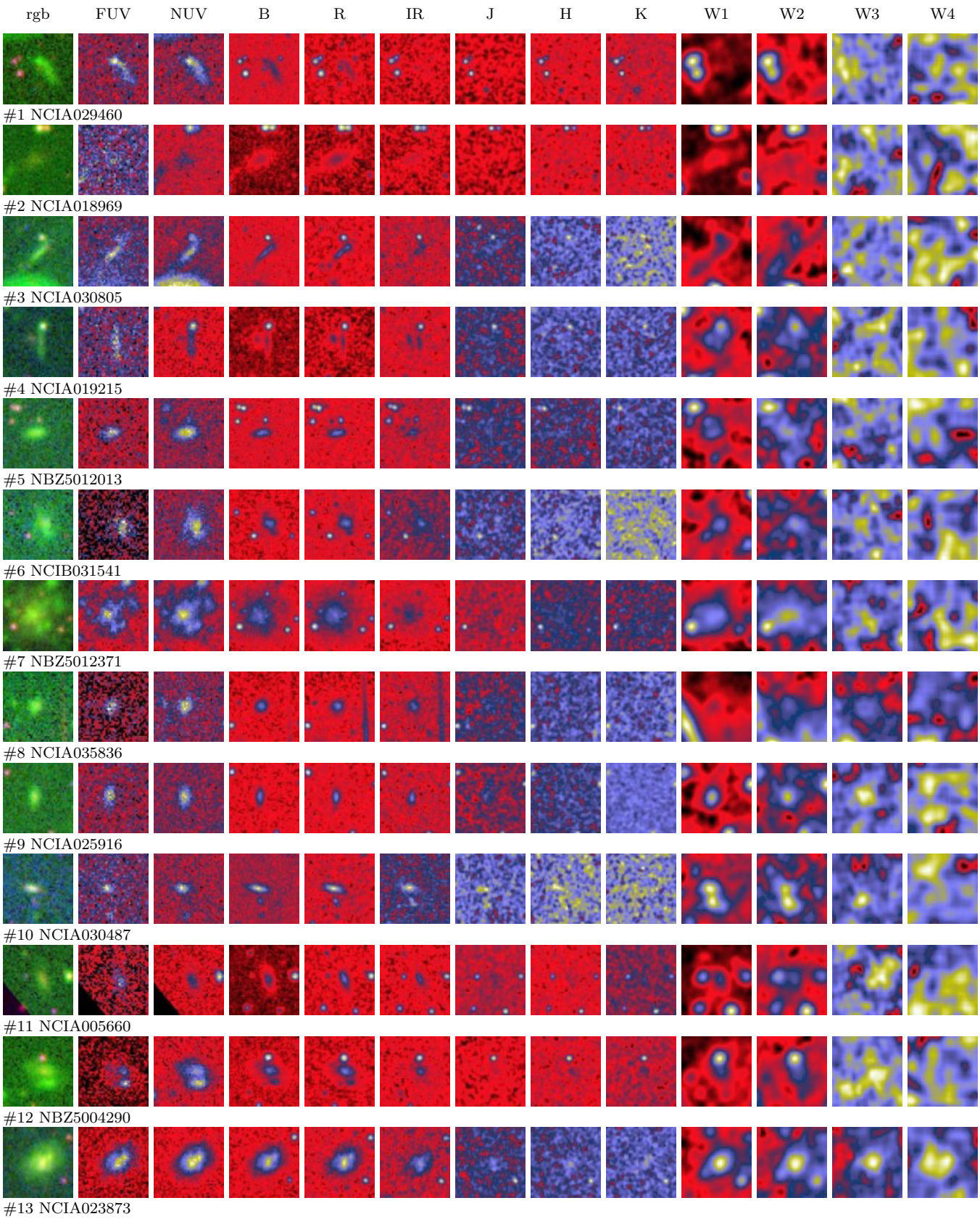

Figure 3. Visible galaxies within 40′ of NGC 891.
(An extended and color version of this figure are available in the online journal.)

emission from the stellar disk. In contrast, none of the dSph galaxies are visible in the *Wise W3* and *W4* bands, which primarily measure emission from dust in the ISM. We take this to mean that these galaxies have been stripped of essentially all gas and dust.

The association of the dSph galaxies with the tidal streams and the signs of disruption near NGC 891 suggest that some or all of the dwarfs might be of tidal origin. This is born out by the appearance of several of the dSph galaxies which appear to be disturbed and "raggedy" with a few seeming to consist of two or three distinct regions. A possible explanation of situation is that the largest dwarf, UGC 1807, had a fly-by interaction with NGC 891 a few Gyr ago and has since recovered so that it now appears to be an undisturbed dI. The other dwarf galaxies are tidal remnants of the original interaction which are bound to NGC 891 and some of this family periodically passes through the plane of NGC 891, disrupting the disk and creating new tidal streams. This scenario is consistent with, for example, Purcell et al. (2011) who suggests that the evolution of galaxy morphology is not entirely secular and that low-mass minor mergers probably have an important role in shaping galactic structure. On the other hand, it is not certain that the dwarf galaxies originated from a single disruption event. For instance, a common origin of many small galaxies in an infalling group or within a large-scale filament the feeds a large galaxy is often given as an explanation of the satellites of the MW and M31.

3.1. UV and NIR Magnitudes

The Aperture Photometry Tool (APT) v2.4.2 (Laher et al. 2012) was used to calculate the apparent magnitude of the galaxies in *WISE* $W1, W2, W3$, and $W4$ bands and in the *GALEX* FUV and NUV bands. The results are given in Table 2. APT is well suited for use in crowded fields in that it is possible to fit an elliptical aperture to a source to avoid nearby stars and because the calculation of the local sky background is not restricted to a simple annulus.

Adjacent *WISE* images id 0364p424_ac51 and id 343p424_ab41, each consisting of 4 images for *W1, W2, W3*, and *W4,* were used to calculate *WISE* magnitudes. The resolution of these images is 1.375 arcsec^{-1} pixel^{-1}. The rectangular images are $93'$ on a side and entirely cover the search region with minimum overlap.

GALEX NUV magnitudes were calculated using one of three overlapping circular images which combine to cover the search region. These are NGA_NGC 0891-nd-int (exposure time = 1704), GI2_019004_3C66B-nd-int (exposure time = 6823 s), and GI5_063003_A347_FIELD1-nd-int (exposure time = 3144 s). Each of the images is $1.^{\circ}25$ in diameter. Even though the first of the three images covers almost all of the search region, the other two images were used when possible because the exposure times were much longer. Cross checking showed that using the longer exposure time resulted in magnitudes which were brighter by about 0.5 mag.

GALEX FUV magnitudes were calculated using two images: NGA_NGC 0891-fd-int(exposure time = 1704) and GI2_019004_3C66B-nd-int (exposure time = 6047 s). Once again, the second image was used preferentially because of the longer exposure time.

Table 2 provides the calculated magnitudes for the 71 galaxies described in Table 1. Table 2 provides the following information:

Column 1: ID number;

Column 2: GSC 2.3.2 ID;

Column 3: *GALEX* FUV apparent magnitude;

Column 4: *GALEX* FUV apparent magnitude;

Column 5: *WISE W1* apparent magnitude;

Column 6: *WISE W2* apparent magnitude;

Column 7: *WISE W3* apparent magnitude;

Column 8: *WISE W4* apparent magnitude;

Column 9: *WISE W1* absolute magnitude assuming a distance of 9.8 Mpc for the "Foreground" galaxies identified in Table 1 and a distance of 75 Mpc for the remaining galaxies;

Column 10: For comparison, *WISE W1* absolute magnitude is provided for the "Foreground" galaxies assuming a distance of 75 Mpc;

Column 11: *WISE W1* luminosity assuming a distance of 9.8 Mpc for the "Foreground" galaxies identified in Table 1 and a distance of 75 Mpc for the remaining galaxies;

Column 12: For comparison, *WISE W1* luminosity is provided for the "Foreground" galaxies assuming a distance of 75 Mpc.

UGC 1807 (ID = 7 in Table 2) is a well-known dIrr galaxy which was found to have a *W1* luminosity of 4.1+08 $L_{\odot}$. The mass-to-light ratio for the *W1* band is near unity and so this implies a mass which is typical of dIrr galaxies. The *W1* luminosity of the remainder of the "Foreground" galaxies ranges from 7.8E+06 to 7.6E+07. This range is typical for dSph galaxies, as discussed in Grebel et al. (2003).

3.2. NIR Surface Brightness versus W1 Magnitude

Figure 5 plots the DSS2 NIR brightness metric which was used to order the candidates of Table 1 versus the *WISE W1* magnitude. The trend is clearly monotonic with a scatter of about 1 mag. This shows that the information in the GSC 2.3.2, although imprecise, could be used to search for low-mass galaxies in an automated process.

A detailed interpretation of Figure 5 is somewhat involved. The trend of the background galaxies is consistent with that shown in Figure 9(a) of Graham & Guzmán (2003) which plots M_B versus $< \mu >_e$ for a large collection of dE and E galaxies which covers the range of values $-23 < M_B < -13$ and $20 < \mu_e < 26$. The single obvious outlying point shown in Figure 5 is the dIrr galaxy UGC 1807 (ID 7 in Table 1). This point is offset from the trend line by the difference in distance mag ($\Delta m \simeq 34$–30) and would lie near the trend line of the background galaxies if all were plotted versus absolute magnitude.

The question arises of why the dwarf galaxies identified in Table 1 are not displaced from the trend line in the same way as UGC 1807. The reason is found in the Figure 2(c) of de Rijcke et al. (2009) which plots M versus μ for many dE's and dSph galaxies. de Rijcke et al. (2009) covers the span of $-24 < M_V < -8$ and the dSph galaxies lie in the range $-14 < M_V < -8$. de Rijcke et al. (2009) find that dSph galaxies do not continue the trend line of dE and E galaxies. The relationship changes slope at about $M_V > 15$ (i.e., at $W1 \sim 15$ at the distance of NGC 891) at which point the slope changes by a factor of slightly more than two. The offset is approximately $\Delta M_V \sim +4$ for galaxies with surface brightness $\mu_{0,V} \sim 25$, which offsets the change due to the different distance mag.

Table 2
GALEX and *WISE* Magnitudes

ID	GSC2.3 ID	FUV mag	NUV mag	*W1* mag	*W2* mag	*W3* mag	*W4* mag	*W1*[a] Mag	*W1*[b] Mag	*W1* L[a] $L_\odot$	*W1* L[b] $L_\odot$
1	NCIA029460	20.4	20.2	16.0	15.6	14.6	11.8	−14.0	−18.4	7.8E+06	4.5E+08
2	NCIA018969	21.4	21.0	15.2	16.4	···	···	−14.8	−19.2	1.7E+07	9.7E+08
3	NCIA030805	20.7	20.5	15.4	15.4	···	13.1	−14.6	−19.0	1.4E+07	8.2E+08
4	NCIA019215	20.9	21.0	15.1	15.7	16.5	···	−14.9	−19.3	1.7E+07	1.0E+09
5	NBZ5012013	19.7	20.0	15.3	14.9	13.8	···	−14.7	−19.1	1.5E+07	8.6E+08
6	NCIB031541	19.2	19.4	15.2	15.3	14.3	···	−14.8	−19.2	1.6E+07	9.2E+08
7	NBZ5012371	17.0	16.7	11.7	11.7	10.8	···	−18.3	−22.7	4.1E+08	2.3E+10
8	NCIA035836	20.2	20.5	14.6	14.6	11.9	11.8	−19.8		1.7E+09	
9	NCIA025916	20.7	20.6	15.0	14.6	11.9	12.2	−19.4		1.1E+09	
10	NCIA030487	21.8	21.1	15.0	15.0	12.9	10.6	−19.4		1.1E+09	
11	NCIA005660	20.2	20.2	15.0	14.8	12.6	12.6	−19.4		1.2E+09	
12	NBZ5004290	18.5	18.4	14.2	14.3	11.9	11.1	−20.2		2.3E+09	
13	NCIA023873	18.4	18.0	13.5	13.5	10.7	8.6	−20.9		4.4E+09	
14	NCIA004638	19.6	19.4	13.9	13.9	11.7	10.0	−20.5		3.0E+09	
15	NBZ5003674	19.2	19.5	14.5	14.5	11.9	12.0	−19.9		1.8E+09	
16	NBZ5015034	20.3	19.9	14.1	14.1	11.6	10.7	−20.3		2.6E+09	
17	NCIA012578	20.8	20.7	14.5	14.7	13.0	10.3	−19.9		1.8E+09	
18	NCIA009669	19.8	19.7	14.4	14.4	11.8	10.0	−20.0		1.9E+09	
19	NCIA010240	20.3	20.2	14.3	14.2	11.3	9.8	−20.1		2.2E+09	
20	NBZ5004664	18.9	18.9	13.1	13.1	10.3	14.5	−21.3		6.4E+09	
21	NCIA007657	20.3	20.6	13.3	13.3	11.3	10.1	−21.1		5.2E+09	
22	NCIA010627	20.6	20.8	14.0	14.0	11.0	11.0	−20.4		2.9E+09	
23	NCIA006643	21.1	22.0	14.7	14.7	15.5	10.9	−19.7		1.6E+09	
24	NCIA010131	20.9	21.0	14.5	14.4	12.8	···	−19.9		1.8E+09	
25	NCIA012182	19.7	19.5	14.1	13.9	11.0	9.9	−20.3		2.6E+09	
26	NCIA012187	20.4	21.3	13.0	12.9	10.1	8.7	−21.4		7.4E+09	
27	NCIA019867	20.6	21.6	13.0	12.8	11.0	11.2	−21.4		7.1E+09	
28	NCIA026109	22.5	22.0	13.8	14.0	13.3	···	−20.6		3.6E+09	
29	NCIA016387	···	19.0	13.1	13.0	10.4	9.2	−21.3		6.7E+09	
30	NCIA031935	20.4	19.9	12.5	12.3	8.7	6.5	−21.9		1.1E+10	
31	NCIA016766	19.3	19.2	13.3	13.2	10.4	9.3	−21.1		5.4E+09	
32	NCIA029870	22.6	21.4	13.0	13.0	13.5	10.3	−21.4		7.4E+09	
33	NCIA010841	19.0	19.0	12.9	12.8	9.5	8.4	−21.5		7.8E+09	
34	NCIA008246	19.7	19.7	13.6	13.6	10.2	8.5	−20.8		4.3E+09	
35	NCIA031681	20.9	20.7	12.5	12.5	10.4	9.6	−21.9		1.1E+10	
36	NCIA010315	18.9	18.6	13.7	13.9	11.2	8.9	−20.7		3.8E+09	
37	NCIA004881	20.5	21.6	12.3	12.3	11.8	10.2	−22.1		1.4E+10	
38	NCIA027059	21.8	21.5	12.7	12.7	12.4	11.3	−21.7		9.9E+09	
39	NCIA031605	21.9	21.6	11.8	11.8	10.4	9.9	−22.6		2.1E+10	
40	NBZ5010876	19.3	18.9	12.8	12.6	9.3	8.1	−21.6		8.8E+09	
41	NCIA027303	21.7	20.7	12.4	12.5	10.8	9.9	−22.0		1.2E+10	
42	NCIA029804	23.0	21.2	12.5	12.5	···	···	−21.9		1.1E+10	
43	NCIA004956	20.5	22.2	12.7	12.7	12.0	···	−21.7		9.8E+09	
44	NCIA006145	20.4	20.6	12.7	12.7	10.9	8.6	−21.7		9.6E+09	
45	NCIA001071	19.0	18.8	12.0	11.9	9.2	7.3	−22.4		1.8E+10	
46	NCIA001356	17.6	17.4	12.1	12.0	8.5	5.8	−22.3		1.6E+10	
47	NCIA015505	20.6	20.2	11.9	11.9	10.3	9.7	−22.5		1.9E+10	
48	NBZ5000254	26.1	19.6	11.8	11.7	9.1	6.9	−22.6		2.1E+10	
49	NCIA000887	18.8	18.5	11.7	11.6	8.8	7.1	−22.7		2.3E+10	
50	NCIA001268	20.4	20.8	12.2	12.2	11.1	11.3	−22.2		1.5E+10	
51	NCIA001160	21.2	20.7	12.4	12.5	12.7	13.9	−22.0		1.2E+10	
52	NCIA000452	20.2	19.5	11.8	11.8	8.8	7.7	−22.6		2.2E+10	
53	NCIA001126	18.6	18.5	11.4	11.3	7.8	6.3	−23.0		3.1E+10	
54	NCIA000277	21.0	20.2	11.7	11.7	10.1	8.7	−22.7		2.4E+10	
55	NCIA001249	20.6	21.6	12.4	12.5	12.4	10.1	−22.0		1.3E+10	
56	NCIA000313	22.1	20.9	11.6	11.6	11.8	10.4	−22.8		2.7E+10	
57	NCIA000956	18.6	18.3	12.1	12.0	8.8	7.5	−22.3		1.6E+10	
58	NCIA030617	22.2	20.8	11.5	11.4	9.9	8.0	−22.9		2.8E+10	
59	NCIA001042	20.2	19.5	11.5	11.4	8.2	5.5	−22.9		2.8E+10	
60	NCIA001337	20.1	20.6	12.1	12.1	12.1	···	−22.3		1.7E+10	
61	NBZ5000678	18.4	18.0	10.5	10.2	6.3	4.4	−23.9		7.2E+10	
62	NBZ5000685	19.0	18.7	11.2	11.2	9.4	8.2	−23.2		3.9E+10	
63	NCIA000991	20.6	20.7	11.6	11.6	11.4	9.6	−22.8		2.6E+10	
64	NCIA000260	21.5	20.5	11.3	11.3	11.2	···	−23.1		3.5E+10	
65	NCIA001051	17.4	16.9	9.8	9.8	7.0	5.5	−24.6		1.4E+11	

Table 2
(Continued)

ID	GSC2.3 ID	FUV mag	NUV mag	*W1* mag	*W2* mag	*W3* mag	*W4* mag	*W1*[a] Mag	*W1*[b] Mag	*W1* L[a] $L_\odot$	*W1* L[b] $L_\odot$
66	NCIA000248	21.3	20.4	11.0	11.1	10.9	12.0	−23.4		4.4E+10	
67	NCIA001220	18.7	18.5	9.2	9.2	7.2	5.9	−25.2		2.4E+11	
68	NCIA000407	19.6	19.2	9.6	9.6	9.3	7.9	−24.8		1.6E+11	
69	NCIA001111	19.7	19.4	10.3	10.3	9.9	9.6	−24.1		9.0E+10	
70	NCIA001162	19.1	18.6	11.3	11.3	8.9	7.6	−23.1		3.5E+10	
71	NCIA000110	20.3	19.3	10.8	10.8	10.4	8.9	−23.6		5.6E+10	

Notes.
[a] Assuming a distance of 9.8 Mpc for foreground galaxies indicated on Table 1 and 75 Mpc for the remainder.
[b] Assuming a distance of 75 Mpc for foreground galaxies for comparison.

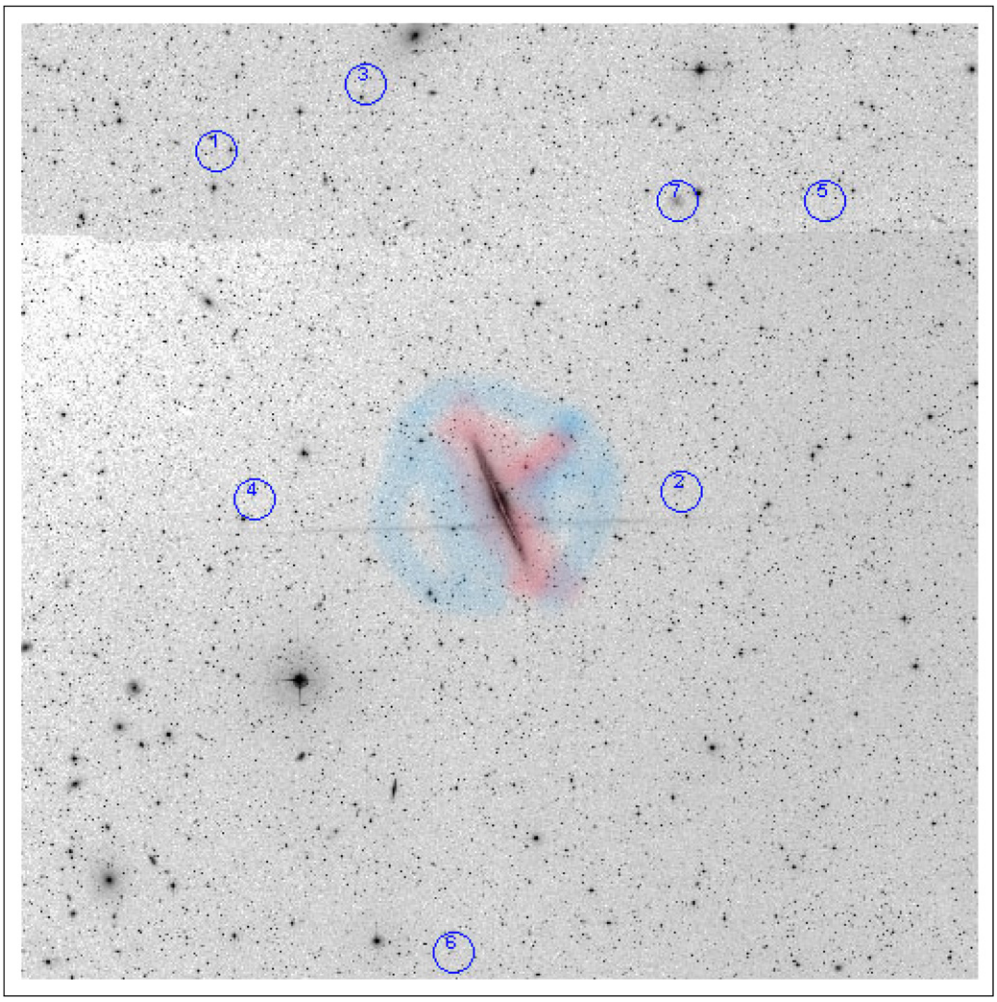

Figure 4. DSS2 *R* image overlaid with the positions of the seven dwarf galaxies identified in this paper using the numbering in Table 1. The scale of this figure is 80′ on a side which is about 228 kpc at the distance of NGC 891. The blue highlighted region is the approximate extent of the streams found in Mouhcine et al. (2010) and the red highlighted region is the approximate extent of the disturbance to the H I surrounding the disk found by the Oosterloo et al. (2007).
(A color version of this figure is available in the online journal.)

3.3. UV Excess

Lee et al. (2011) reports that the ratio of *GALEX* UV to 2MASS *K* magnitude is much higher for galaxies which are dim in I_N and also that detection in UV is more reliable for dSph and dIrr galaxies than detection in the *B* or *R* bands. Similarly, Lee et al. (2009) reports that the FUV-to-H_α ratio is larger than expected, especially for lower luminosity dwarf galaxies. The FUV/H_α and NUV/H_α ratios of the lowest luminosity galaxies are larger than expected by an order of magnitude or more compared to larger galaxies.

Buat et al. (2005) compared a NUV-selected sample of galaxies to a FIR-selected sample and found that the average dust attenuation of the NUV-selected sample was 0.8, whereas the average attenuation of the FIR sample was 2.1 and was larger than about 5.0 for some galaxies not detected in FUV.

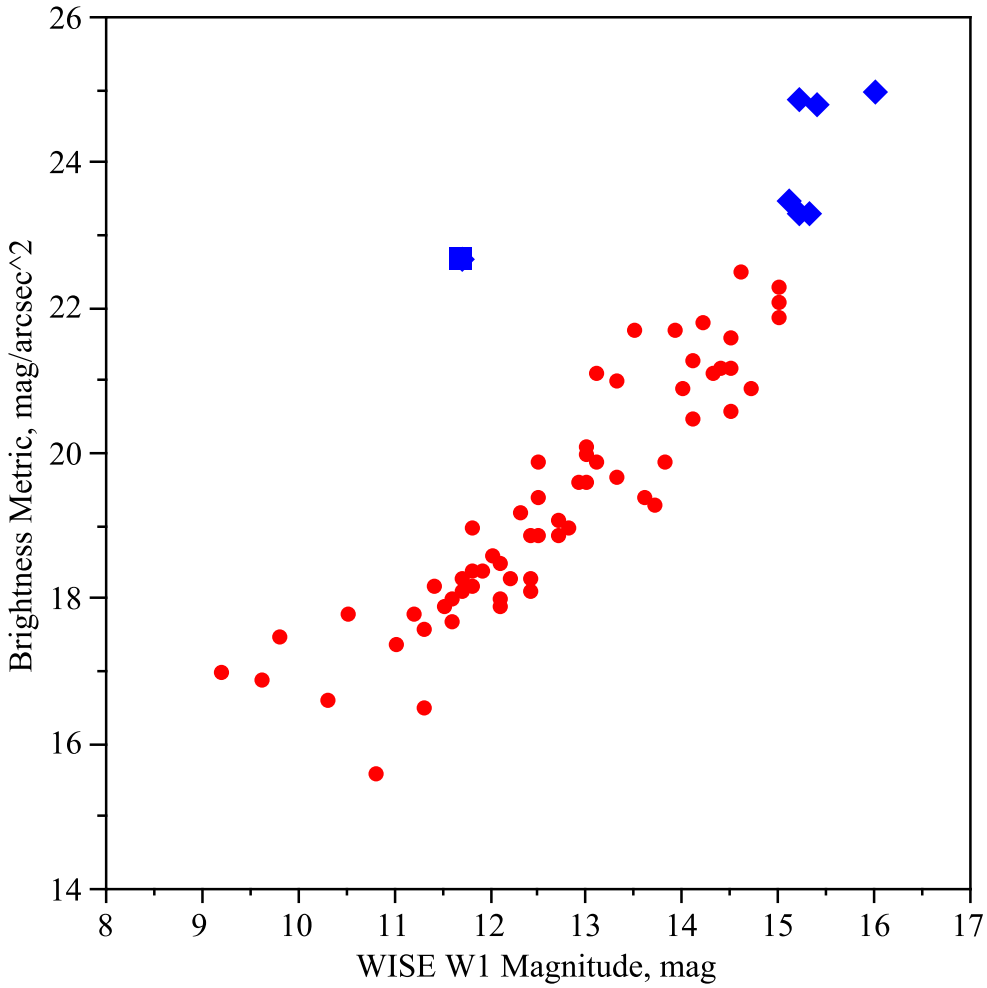

Figure 5. Brightness parameter NIR μ is based on the GSC 2.3.2 NIR magnitude and size. The red circles mark background galaxies, the single solid blue box marks the foreground dIrr UGC 1807, and the solid blue diamonds mark foreground dSph galaxies as identified in Table 1. The background galaxies exhibit a smooth function of NIR μ vs. the *WISE W1* apparent magnitude which is a proxy for mass for these galaxies at the same distance. The foreground dIrr follows the same trend as the background galaxies but is offset because of distance. Despite appearances, the foreground dSph galaxies do not follow the trend of the background galaxies. The curve flattens for these low-mass galaxies but the change of slope is offset by the effect of the very different distances of the two populations.

(A color version of this figure is available in the online journal.)

Strikingly, they found a cutoff so that there is *no* dust attenuation in the NUV band for galaxies with luminosity less than about $5\times10^8\ L_\odot$, i.e., the dSph galaxies.

Cortese et al. (2008) modeled the dependance of the attenuation of galaxy FUV emissions, A (FUV), to the ratio of total IR emission (TIR) to FUV and to the age of the underlying stellar distribution. They find that A (FUV) increases dramatically as the TIR/FUV ratio increases and also increases as the age of the underlying stellar population increases, especially from 3 Gyr to 4 Gyr. The FUV attenuation can be as large as several mags but is negligible, and age is not significant, for galaxies with a small TIR/FUV ratio.

This effect was seen in the present study and is strong enough to help distinguish foreground dSph galaxies from background galaxies. All of the identified dSph galaxies are confirmed in NUV and in FUV and none are visible in 2MASS *J*, *H*, or *K*. The UV excess of the dSph galaxies shown in Figure 3 is estimated to be more than two magnitudes compared to background galaxies.

Figure 6 plots *GALEX* NUV–*WISE W1* versus *W1* magnitude. This figure clearly shows that there is a strong trend of NUV excess with decreasing mass.

The present results are consistent with Buat et al. (2005) and suggest that the observed UV excess is due to the absence of gas and dust in the dSph galaxies. In normally sized galaxies, most of the UV emitted by stars in the observed galaxy is absorbed locally by dust and re-emitted in NIR. In contrast, the UV emitted by the stars of the dust-free dSph galaxies is observed with very little attenuation and the NIR emission is negligible. Note, however, that Lee et al. (2009) argues the contrary and asserts that dust attenuation effects cannot explain the UV excess.

Again 6 includes galaxies which are at very different distances and so the apparent *W1* magnitude is not a proxy for mass.

3.4. Completeness

Lasker et al. (2008) claims that the GSC 2.3 includes "almost all" of the objects down to the plate limits which are $B_J < 22.5$, $R_F < 20.8$, and $I_N < 19.5$. Table 1 is complete to these plate limits with the added constraint on size of $D > 15''$.

With one exception, the survey found all of the previously cataloged galaxies in the search region which met the size limit. This good result implies that the current survey is complete to the plate accuracy of the DSS2. The single exception was that we were unable to verify the dSph galaxy [TT2009]30 reported by Trentham & Tully (2009). This good result demonstrates that

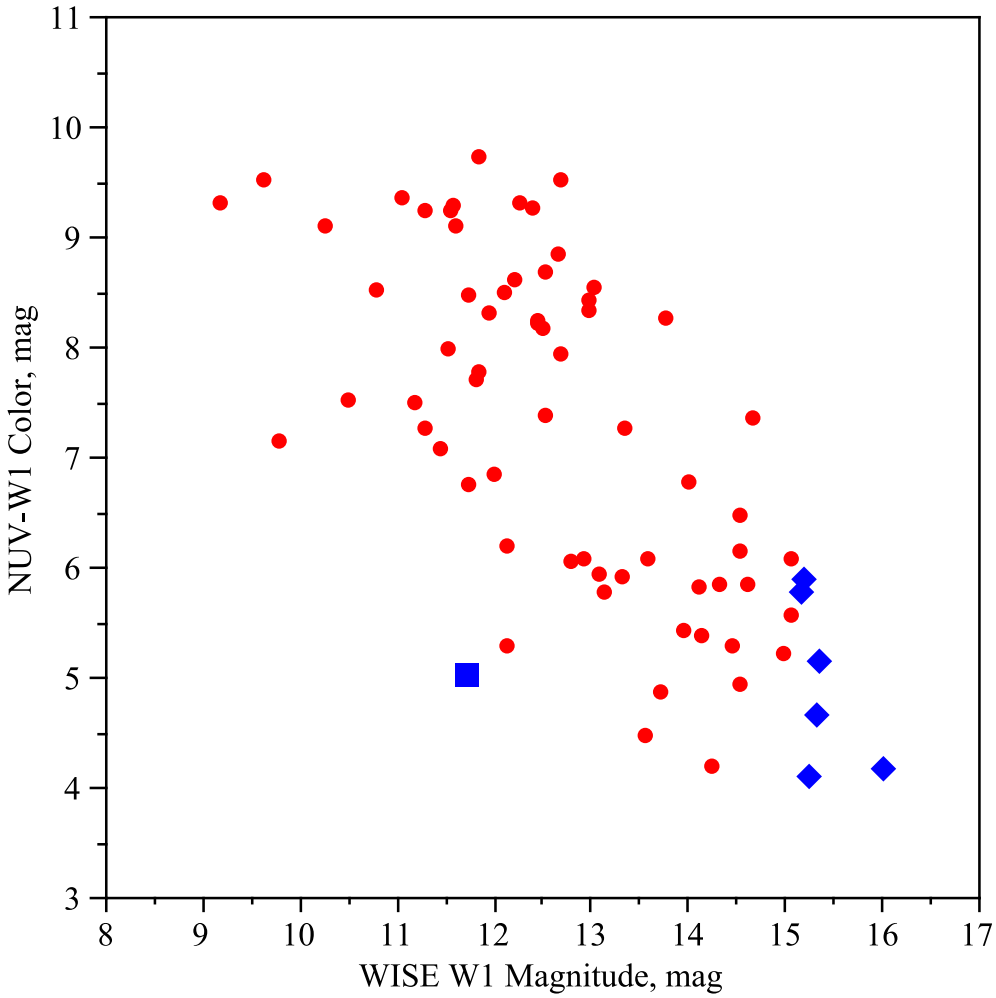

Figure 6. *Galex* NUV—*Wise W1* plotted vs. *W1* apparent magnitude. The red circles mark background galaxies, the single solid blue box marks the foreground dIrr UGC 1807, and the solid blue diamonds mark foreground dSph galaxies as identified in Table 1. The trend of the background galaxies show that there is a large UV excess for low-mass galaxies in comparison to higher mass galaxies. The large scatter in this relation is due to the real effect of differences in SFR, not measurement error. The foreground dIrr follows the same trend as the background galaxies but is offset because of distance. Despite appearances, the foreground dSph galaxies do not follow the trend of the background galaxies. The curve flattens for these low-mass galaxies but the change of slope is offset by distance.

(A color version of this figure is available in the online journal.)

the current survey is complete in the target region to within the defined size limit.

4. SUMMARY

We report the results of a size-limited survey of the region near NGC 891. Seventy-one galaxies with apparent diameters less than 15″ were found in the region $R \leqslant 40'$ around NGC 891. Seven of these galaxies were identified as likely dwarf galaxies in the halo of NGC 891 and several others are likely candidates. Most of the remaining galaxies are members of the A347 cluster, which approximately doubles the known membership of the cluster.

Although the present survey reports an increase in the number of dwarf galaxies near NGC 891 the number of new discoveries falls far short of that needed to account for the "missing satellites" discussed above. This evidence supports the current status based on counts of the dwarf companions of the MW that there is a basic conflict between observations and the accepted theory of galaxy formation.

The methodology described here of examining candidates taken from the Guide Star Catalog in several different bands is much more efficient and thorough than previous surveys of the region. Searches which depend on a single band, especially near the Galactic plane, are plagued by contamination, diffraction effects, and various sorts of artifacts which are easily eliminated when the same region is viewed at many wavelengths.

The Guide Star Catalog II is a joint project of the Space Telescope Science Institute and the Osservatorio Astronomico di Torino. The Digitized Sky Surveys were produced at the Space Telescope Science Institute under U.S. Government grant NAG W-2166. The images of these surveys are based on photographic data obtained using the Oschin Schmidt Telescope on Palomar Mountain and the UK Schmidt Telescope.

This publication makes use of data products from the Two Micron All Sky Survey, which is a joint project of the University of Massachusetts and the Infrared Processing and Analysis Center/California Institute of Technology.

This research has made use of the Aladin interactive sky atlas, developed at CDS, Strasbourg, France.

We acknowledge the use of NASA's SkyView virtual observatory (McGlynn et al. 1998)

This research has made use of the VizieR catalogue access tool, CDS, Strasbourg, France.

This research has made use of the NASA/IPAC Extragalactic Database (NED) which is operated by the Jet Propulsion Laboratory, California Institute of Technology, under contract with the National Aeronautics and Space Administration.

We also gratefully acknowledge use of Figure 1 of Mouhcine et al. (2010). The author gratefully acknowledges the anonymous referee whose comments and suggestions greatly improved the quality of the paper.

REFERENCES

Barkana, R., & Loeb, A. 1999, ApJ, 523, 54
Boylan-Kolchin, M., Bullock, J. S., & Kaplinghat, M. 2011, MNRAS, 415, L40
Boylan-Kolchin, M., Bullock, J. S., & Kaplinghat, M. 2012, MNRAS, 422, 1203
Buat, V., Iglesias-Páramo, J., Seibert, M., et al. 2005, ApJL, 619, L51
Bullock, J. S., Stewart, K. R., Kaplinghat, M., Tollerud, E. J., & Wolf, J. 2010, ApJ, 717, 1043
Conselice, C. J., Gallagher, J. S., III, & Wyse, R. F. G. 2002, AJ, 123, 2246
Cortese, L., Boselli, A., Franzetti, P., et al. 2008, MNRAS, 386, 1157
de Rijcke, S., Penny, S. J., Conselice, C. J., Valcke, S., & Held, E. V. 2009, MNRAS, 393, 798
Dekel, A., & Silk, J. 1986, ApJ, 303, 39
Gallagher, J. S., III, & Wyse, R. F. G. 1994, PASP, 106, 1225
Gil de Paz, A., Boissier, S., Madore, B. F., et al. 2007, ApJS, 173, 185
Grcevich, J., & Putman, M. E. 2009, ApJ, 696, 385
Grebel, E. K., Gallagher, J. S., III, & Harbeck, D. 2003, AJ, 125, 1926
Guo, Q., White, S., Li, C., & Boylan-Kolchin, M. 2010, MNRAS, 404, 1111
Graham, A. W., & Guzmán, R. 2003, AJ, 125, 2936
Hau, G. K. T., Ferguson, H. C., Lahav, O., & Lynden-Bell, D. 1995, MNRAS, 277, 125
Huchra, J. P., Macri, L. M., Masters, K. L., et al. 2012, ApJS, 199, 26
Huchtmeier, W. K., Karachentsev, I. D., & Karachentseva, V. E. 2009, A&A, 506, 677
Jarrett, T. H., Chester, T., Cutri, R., et al. 2000, AJ, 119, 2498
Kaisina, E. I., Makarov, D. I., Karachentsev, I. D., & Kaisin, S. S. 2012, AstBu, 67, 115
Karachentsev, I. D., & Kaisin, S. S. 2010, AJ, 140, 1241
Karachentsev, I. D., Karachentseva, V. E., & Huchtmeier, W. K. 2007, AstL, 33, 512
Karachentsev, I. D., Karachentseva, V. E., Huchtmeier, W. K., & Makarov, D. I. 2004, AJ, 127, 2031
Klypin, A., Kravtsov, A. V., Valenzuela, O., & Prada, F. 1999, ApJ, 522, 82
Laher, R. R., Gorjian, V., Rebull, L. M., et al. 2012, PASP, 124, 737
Larson, R. B. 1974, MNRAS, 169, 229
Lasker, B. M., Lattanzi, M. G., McLean, B. J., et al. 2008, AJ, 136, 735
Lee, J. C., Gil de Paz, A., Kennicutt, R. C., Jr., et al. 2011, ApJS, 192, 6
Lee, J. C., Gil de Paz, A., Tremonti, C., et al. 2009, ApJ, 706, 599
Martin, D. C., Fanson, J., Schiminovich, D., et al. 2005, ApJL, 619, L1
Martínez-Delgado, D., Gabany, R. J., Crawford, K., et al. 2010, AJ, 140, 962
McConnachie, A. W. 2012, AJ, 144, 4
McGlynn, T., Scollick, K., & White, N. 1998, in IAU Symp. 179, New Horizons from Multi-Wavelength Sky Surveys, ed. B. J. McLean, D. A. Golombek, J. J. E. Hayes, & H. E. Payne (Cambridge: Cambridge Univ. Press), 465
Moore, B., Ghigna, S., Governato, F., et al. 1999, ApJL, 524, L19
Mouhcine, M., Ibata, R., & Rejkuba, M. 2010, ApJL, 714, L12
Nichols, M., & Bland-Hawthorn, J. 2011, ApJ, 732, 17
Oosterloo, T., Fraternali, F., & Sancisi, R. 2007, AJ, 134, 1019
Purcell, C. W., Bullock, J. S., Tollerud, E. J., Rocha, M., & Chakrabarti, S. 2011, Natur, 477, 301
Sakai, S., Kennicutt, R. C., & Moss, C., Jr. 2012, ApJS, 199, 36
Shih, H., & Méndez, R. H. 2010, ApJL, 725, L97
Skrutskie, M. F., Cutri, R. M., Stiening, R., et al. 2006, AJ, 131, 1163
Tikhonov, N. A., & Galazutdinova, O. A. 2005, Ap, 48, 221
Trentham, N., & Tully, R. B. 2009, MNRAS, 398, 722
White, S. D. M., & Frenk, C. S. 1991, ApJ, 379, 52
White, S. D. M., & Rees, M. J. 1978, MNRAS, 183, 341
Whiting, A. B., Hau, G. K. T., Irwin, M., & Verdugo, M. 2007, AJ, 133, 715
Wright, E. L., Eisenhardt, P. R. M., Mainzer, A. K., et al. 2010, AJ, 140, 1868